Seismic Characterization of the Chelyabinsk Meteor's Terminal Explosion

by Sebastian Heimann, Álvaro González, Rongjiang Wang, Simone Cesca, and Torsten Dahm

Online Material: Figures of waveform fit, apparent source time functions, and video of impact of shock wave at factory.

INTRODUCTION

Impacts with our planet cause seismic shaking by a variety of mechanisms. Catastrophic ground motion, even at antipodal distances, can be generated by the extremely infrequent, hypersonic collisions with large asteroids or comets (Meschede *et al.*, 2011). Fortunately, the atmosphere effectively shields the smaller (and far more common) meteoroids, greatly reducing their initial kinetic energy at high altitude, causing them to slow down, break up, and even vaporize, producing a meteor (Ceplecha and Revelle, 2005). In most instances, the ground shaking is triggered by the atmospheric shock wave of a meteor, not by the impact of the surviving meteorites (Edwards *et al.*, 2008).

A particularly strong shock wave can be generated by explosive fragmentation of the meteoroid in one or several final airbursts (Ceplecha and Revelle, 2005; Edwards *et al.*, 2008). Such disruptions are triggered when the pressure (ram pressure) caused by atmospheric drag exceeds the internal strength of a meteoroid. They are accompanied by a sudden increase in the meteor luminosity (a flare), because they imply a sharp increase in the surface area being subject to ablation.

On 15 February 2013 at 03:20 UTC, an exceptionally large meteor in the region of Chelyabinsk, Russia, produced a powerful shock wave, which caused unprecedented damage to people and property. According to official news reports, glass windows were shattered in over 7300 buildings (some of these even experienced slight structural damage), and falling debris hurt more than 1600 people. The meteorite fragments that survived the atmospheric entry hit the ground at subsonic terminal velocity (Schiermeier, 2013), and did not cause any seismic shaking detectable at regional distances. However, the meteor produced the strongest atmospheric infrasound signal ever recorded (Stone, 2013) and remarkable ground motion, which is the topic of this paper.

Here we describe and model the resulting seismic surface waves, observed at distances of over 4000 km. Our modeling indicates that the ground shaking was caused by the terminal explosion (airburst) of the meteor southwest of Chelyabinsk city, and had an equivalent moment magnitude of 3.60. This implies that this is the second largest meteor explosion ever seismically recorded, only surpassed by the 1908 Tunguska event (Ben-Menahem, 1975).

DESCRIPTION OF THE GROUND SHAKING

The seismic ground shaking caused by the Chelyabinsk meteor was exceptionally well registered at planetary scale. It can be observed in more than 70 digital, broadband seismic recordings from stations located at least up to 4000 km away, sampling most azimuths. At further distances, the identification of the meteor signal is hampered by the coincidental interference with wave arrivals from a tectonic earthquake with magnitude M_w 5.7, originated in Tonga at 03:02:23 UTC. In comparison, when the 1908 Tunguska meteor explosion took place, seismic monitoring was in its infancy; the resulting surface waves were observed only in four seismic stations up to 5300 km away (Ben-Menahem, 1975).

The ground shaking caused by the Chelyabinsk meteor is dominated by Rayleigh waves. Clearly visible both on the vertical and radial components of the displacement records, they travel at up to 3.9 km s^{-1}. These surface waves can be excited below a meteor when its atmospheric shock wave hits the ground (Edwards *et al.*, 2008). In this case, the shock wave was able to generate broadband Rayleigh waves, with most energy released at about 0.04 Hz. This dominant frequency is related to the resonance of the Earth's crustal structure. Unlike tectonic earthquakes or underground explosions, the body waves are almost absent, and sharp onsets cannot be identified even at the closest station, ~220 km away. Almost no seismic energy is detected above 0.1 Hz, or on transversal components, in contrast to tectonic earthquakes with similar seismic moment.

SOURCE INVERSION BY FULL WAVEFORM FITTING

We determined the parameters of the Chelyabinsk seismic source, modeling it for simplicity as an isotropic atmospheric airburst. The lack of sharp wave arrivals for this event hampers

doi: 10.1785/0220130042

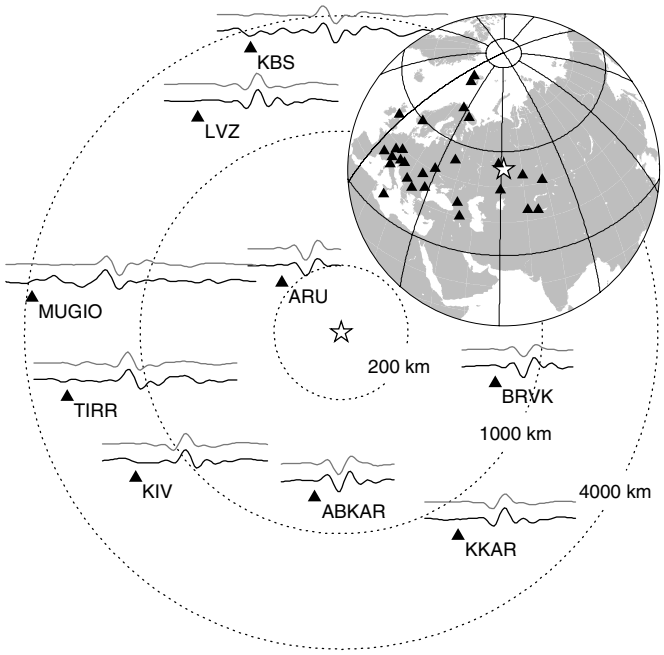

▲ **Figure 1.** Examples of waveform fits at different distances and azimuths around the meteor explosion. Triangles, seismic stations used for the analysis. Black traces, observed seismograms. Gray traces, synthetic ones. Star, explosion source. For the complete set of station codes, seismograms, and synthetic fits, see Ⓔ Figure S1 in the supplement.

location techniques based on them (e.g., its USGS epicenter is located more than 30 km north of the meteor ground path), so we performed a full-waveform inversion. Our seismogram simulation code was tailored to consider wave propagation in the atmosphere and solid Earth, and the coupling at the interface between them (Wang, 2010; applied by Raveloson *et al.*, 2012). It considers a spherically symmetric, viscoelastic, self-gravitating Earth, with seismic velocities specified by the global model AK135Q (Kennett *et al.*, 1995), and atmospheric sound velocities from a standard model (Committee on the Extension of the Standard Atmosphere, 1976).

Synthetic Rayleigh waves for a range of possible times, epicentral locations, and explosion altitudes up to 50 km were generated to simulate the observed 28 vertical and 6 radial high-quality displacement seismograms at 28 broadband seismic stations up to a distance of ~4100 km (Fig. 1; and Ⓔ Fig. S1, available in the electronic supplement to this paper). We chose to fit the seismograms in the frequency range 0.005–0.025 Hz (periods from 40 to 200 s), because within it the seismic signals are not significantly modified by lateral heterogeneities of the Earth's atmosphere and crustal structure. For the modeling we assume a 5 s boxcar source time function, which is effectively point-like in time in the frequency range analyzed. The source-parameter optimization minimizes the misfits between the observed and synthetic traces, computed according to a L1 norm (e.g., Edwards *et al.*, 2008); uncertainties were estimated through bootstrap (e.g., Press *et al.*, 1992, as implemented by Heimann, 2011).

The best-fitting epicenter is found 32 km south-southwest of Chelyabinsk city, exactly in the terminal, most luminous part of the meteor trajectory, around which the shock-wave damage was observed (Table 1 and Fig. 2). The depicted ground path of the meteoroid is based on eyewitness observations and videos, U.S. Government satellite sensor data (Chesley, 2013), and the location of the meteorite-strewn field at Lake Chebarkul and surroundings. In particular, a major meteorite fragment splashed in this frozen lake, punching a hole ~6 m in diameter, exactly at 54.95966° N, 60.32074° E. We determined these coordinates from public pictures of the site and satellite imagery (by DigitalGlobe, taken 16 February 2013).

The epicentral location is relatively accurate, considering that it is based only on seismic observations at regional distances, without any station in the immediate vicinity of the meteor. The meteoroid speed of about 18.6 km s^{-1} (Yeomans, 2013) places an intrinsic limitation to the location accuracy. The explosion altitude is poorly resolved by seismic data alone at large distances, because the Rayleigh-wave excitation mechanism is almost independent of explosion height in the observed frequency range. These seismic observations themselves are able to constrain the arrival of the shock wave to the ground, but not its atmospheric travel time.

Table 1
Source Parameters Calculated for the Meteor Explosion at Unconstrained Origin Time and with Origin Time Equal to the Moment of Peak Meteor Brightness

	Unconstrained Origin Time		Fixed Origin Time	
Parameter	**Value**	**68% Confidence Interval**	**Value**	**68% Confidence Interval**
Longitude	61.22	[60.99, 61.30] [−15 km, +5 km]	Same as unconstrained	
Latitude	54.88	[54.65, 55.01] [−25 km, +15 km]	Same as unconstrained	
Altitude	>0	[0, ~50]	22.5 km	[21.0, 24.0]
Magnitude (M_w)		[3.1, 4.0]	3.60	[3.57, 3.62]
Origin time (hh:mm:ss)		[03:19:02, 03:21:43] UTC	03:20:33 UTC (fixed)	

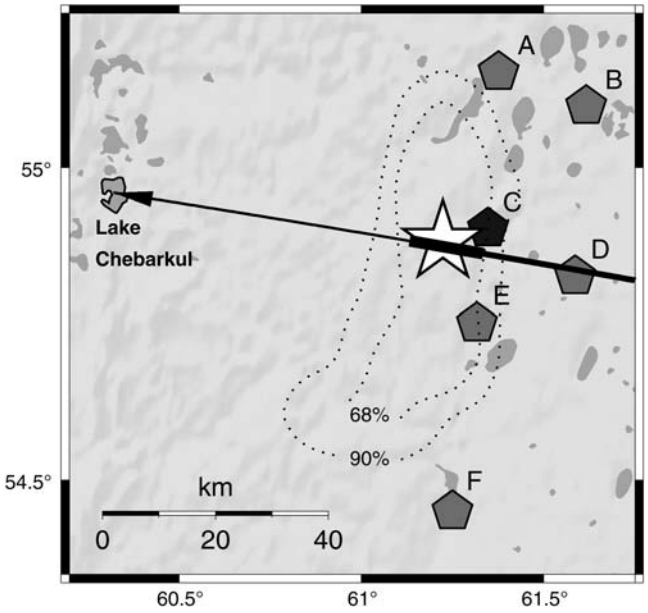

▲ **Figure 2.** Seismic source, terminal meteor trajectory, and distribution of shock-wave damage. Star, our optimally fitting epicenter, with contours indicating the confidence regions (for unconstrained origin time); pentagons, the most damaged population centers (Russian Ministry of Internal Affairs, 2013): (A) Chelyabinsk, (B) Kopeysk, (C) Korkino, (D) Etkul', (E) Yemanzhelinsk, and (F) Yuzhnouralsk. Lakes are shown in gray (after Lehner and Döll, 2004). The arrow depicts the terminal part of the approximate meteoroid ground path. Past Korkino (black pentagon), the meteor had its brightest flare (coincident with the seismic explosion source), after which it faded abruptly and eventually vanished (thin trace).

On the seismic records, we do not find evidence of a preferential direction of the shock wave. This anisotropy, if present, should be manifested by azimuthal variations in the arrival times (e.g., Edwards *et al.*, 2008), amplitude, duration, or dominant frequencies. Instead, the records are azimuthally homogeneous in the analyzed frequency range (as shown, for example, by the apparent source time functions, Ⓔ Fig. S2; see supplement). Overall, an isotropic point-like airburst reproduces very well these seismic observations, without requiring a more complex explanation, such as a moving source. This indicates that, as in some other cases (Edwards *et al.*, 2008), only the shock wave from the meteor outburst was strong enough to excite the measured seismic shaking, at least at the distances from which there is seismic record. In contrast, the atmospheric infrasound signals radiating from a stretch of the trajectory of a large meteor can be strong enough to be detected at long distances and to indicate a moving, hypersonic source (e.g., Edwards, 2010).

The calculated moment magnitude decreases with the modeled explosion altitude. For example, a source with M_w 3.3 at 40 km altitude produces the same seismic amplitudes in the modeled seismograms as another source at 10 km with M_w 3.8. The reason is that, for an atmospheric explosion, $M_0 \propto \sqrt{\rho}$ (assuming constant sound speed) in which M_0 is the seismic moment and ρ is the air density (which decreases with altitude).

If the explosion had been underground, we calculate that a much higher moment magnitude (M_w 4.8 for a source at 1 km depth) would be required to generate the large-amplitude Rayleigh waves observed. For comparison, we observed that (in the same frequency band and at comparable distances) Rayleigh waves excited by the Chelyabinsk meteor had amplitudes about three times larger than those produced by the North Korean nuclear underground explosion (M_w 4.5) three days earlier.

REFINEMENTS BASED ON THE AIRBURST ORIGIN TIME

To calculate the airburst altitude and the precise moment magnitude, we use the timing of the peak meteor brightness as an independent constraint. The most luminous flare, with apparent brightness larger than the Sun's (Brown, 2013), took place at 03:20:33 UTC (Yeomans, 2013). Using this as the origin time of the airburst, we calculate an airburst altitude of 22.5 ± 1.5 km (Table 1), in agreement with independent, preliminary estimates of 23.3 km of the meteor altitude at peak brightness (Yeomans, 2013).

The shock wave generated by a meteoroid entry or explosion is initially hypersonic, and slows to acoustic wave speeds after travelling a few tens to hundreds of meters away from the meteoroid trajectory (Edwards *et al*, 2008). Our calculations omit this nonlinear effect, and assume that the shock wave travels at acoustic speed. Considering that the speed is initially faster would yield a slightly higher source altitude (e.g., Edwards and Hildebrand, 2004).

In turn, using a more realistic atmospheric profile (e.g., Edwards and Hildebrand, 2004; Arrowsmith *et al.*, 2007) for the Chelyabinsk region would tend to yield slightly lower source altitudes. This is because the temperature (at least near the ground) was lower than assumed by the standard atmospheric model (at the airport of Chelyabinsk–World Meteorological Organization observatory ID 28645, it was −21.8° C at 3:00 UTC), which implies slower sound speeds.

Nevertheless, the most important source of altitude uncertainty is the hypersonic vertical component of the meteoroid speed (−2.4 km s^{-1}; Yeomans, 2013). Because of it, further constraining the source altitude would require subsecond accuracy of the timing of peak brightness. Overall, the uncertainties imply an error range of a few km in altitude, as demonstrated by the modeling results (Table 1).

Constraining the origin time allows a precise estimate of the moment magnitude of the ground shaking: M_w 3.60 (Table 1). This value (or the M_w 4.8 for an assumed shallow explosion source) is the second largest ever recorded for a meteor, only surpassed by the $M_w \sim 5.0$ of Tunguska (Ben-Menahem, 1975).

VALIDATION OF THE SOURCE LOCATION WITH A VIDEO RECORDING

The Chelyabinsk meteor was recorded in dozens of casual or surveillance videos and associated audio. They lack exact timing, a common problem faced when trying to characterize meteor trajectories (Gural, 2012), but a few of them can be useful for estimating atmospheric travel times of the shock wave.

We use a particularly valuable surveillance video (Ⓔ see supplement S3), showing the direct shock-wave arrival to Korkino (the town closest to the brightest meteor flare; Fig. 2) to provide an independent validation of the explosion location. It was recorded inside a corrugated carton factory located at 61.347° E, 54.902° N. We measured the building orientation in a detailed map, and inspected the video frame by frame. The windows facing south-southeast (N169°E), toward the meteor trajectory, were smashed by the shock wave 87.5 s after the apparent peak meteor brightness.

The travel time of the shock wave from the explosion source to this building (calculated from our simulation code with the origin time fixed as before) is 88 s, with a 68% uncertainty range of [82–118] s, due to the uncertainties in the source location and altitude. Thus, this video recording supports the preferred estimate of the explosion location.

CONCLUSIONS

The Chelyabinsk meteor experienced a major terminal explosion, manifested as the flare with peak brightness. The resulting atmospheric shock wave caused the damage observed around the explosion source (Fig. 2). Seismic shaking was generated by direct coupling of the atmospheric shock wave with the ground, and recorded hundreds to thousands of kilometers away (Fig. 1). This terminal explosion took place in the stratosphere, at an altitude of ~23 km. Had it occurred at a lower altitude, its shock wave could have been even more damaging. It had an equivalent M_w 3.60, implying that the Chelyabinsk meteor explosion was the second largest ever seismically recorded, only surpassed by the Tunguska event.

Our results highlight that distant seismic recordings can agree remarkably well with local meteor observations, and herald the potential for characterizing future large meteors with scarce direct data. This could be particularly useful in remote areas or above the oceans, and potentially also for fast location and early warning. That most of the seismic energy of the meteor was released from a terminal explosion highlights the danger posed by such phenomena, and we hope that this study would help increase public awareness.

We expect that our seismic analysis could be used as a basis of more detailed reconstructions of the Chelyabinsk meteor, which potentially will benefit from other imagery, eyewitness chronicles, and modeling of signals recorded in infrasound stations worldwide.

POSTSCRIPT

After this manuscript was accepted for publication, other papers related to the Chelyabinsk meteor have been published. Particularly, Tauzin *et al.* (2013) made a seismic analysis complementary to ours, and Le Pichon *et al.* (2013) presented the first results of the infrasound records.

ACKNOWLEDGMENTS

We acknowledge all the seismographic institutions and the Incorporated Research Institutions for Seismology (IRIS) consortium for providing the seismograms, the Internet community for contributing with videos and eyewitness reports, and an anonymous reviewer for valuable comments. The surveillance video was kindly provided by YuzhUralKarton, LLC, thanks to Dan Chernovalov. The figures were elaborated using Generic Mapping Tools (Wessel and Smith, 1998). Á. G. is supported by a grant of Caja Madrid Foundation (Spain) and the Spanish Government project FIS2010-19773. S. C. is supported by the German Federal Ministry of Education and Research (BMBF) project MINE.

REFERENCES

Arrowsmith, S. J., D. P. Drob, M. A. H. Hedlin, and W. Edwards (2007). A joint seismic and acoustic study of the Washington State bolide: Observations and modeling, *J. Geophys. Res.* **112,** D09304, doi: 10.1029/2006JD008001.

Ben-Menahem, A. (1975). Source parameters of the Siberian explosion of June 30, 1908, from analysis and synthesis of seismic signals at four stations, *Phys. Earth Planet. In.* **11,** 1–35, doi: 10.1016/0031-9201(75)90072-2.

Brown, P. (2013). A preliminary report on the Chelyabinsk fireball/airburst, *J. Int. Meteor Organ.* **41,** 22.

Ceplecha, Z., and D. O. Revelle (2005). Fragmentation model of meteoroid motion, mass loss, and radiation in the atmosphere, *Meteoritics Planet. Sci.* **40,** 35–54, doi: 10.1111/j.1945-5100.2005.tb00363.x.

Chesley, S. (2013). Chelyabinsk impactor ground track, in D. Yeomans and P. Chodas, *Additional Details on the Large Fireball Event over Russia on Feb. 15, 2013*, National Aeronautics and Space Administration, http://neo.jpl.nasa.gov/news/fireball_130301.html (last accessed 15 June 2013).

Committee on the Extension of the Standard Atmosphere (1976). *U.S. Standard Atmosphere 1976*, U.S. Government Printing Office, Washington, D.C.

Edwards, W. N. (2010). Meteor generated infrasound: Theory and observation, in A. Le Pichon, E. Blanc, and A. Hauchecorne (Editors), *Infrasound Monitoring for Atmospheric Studies*, Springer, Dordrecht, Netherlands, 361–414.

Edwards, W. N., and A. R. Hildebrand (2004). SUPRACENTER: Locating fireball terminal bursts in the atmosphere using seismic arrivals, *Meteoritics Planet. Sci.* **39,** 1449–1460, doi: 10.1111/j.1945-5100.2004.tb00121.x.

Edwards, W. N., D. W. Eaton, and P. G. Brown (2008). Seismic observations of meteors: Coupling theory and observations, *Rev. Geophys.* **46,** RG4007, doi: 10.1029/2007RG000253.

Gural, P. S. (2012). A new method of meteor trajectory determination applied to multiple unsynchronized video cameras, *Meteoritics Planet. Sci.* **47,** 1405–1418, doi: 10.1111/j.1945-5100.2012.01402.x.

Heimann, S. (2011). A Robust Method to Estimate Kinematic Earthquake Source Parameters, *Ph.D. Thesis*, University of Hamburg,

available at http://ediss.sub.uni-hamburg.de/volltexte/2011/5357/ (last accessed 6 September 2013).
Kennett, B. L. N., E. R. Engdahl, and R. Buland (1995). Constraints on seismic velocities in the Earth from traveltimes, *Geophys. J. Int.* **122,** 108–124, doi: 10.1111/j.1365-246X.1995.tb03540.x.
Lehner, B., and P. Döll (2004). Development and validation of a global database of lakes, reservoirs and wetlands, *J. Hydrol.* **296,** 1–22, doi: 10.1016/j.jhydrol.2004.03.028.
Le Pichon, A., L. Ceranna, C. Pilger, P. Mialle, D. Brown, P. Herry, and N. Brachet (2013). The 2013 Russian fireball largest ever detected by CTBTO infrasound sensors, *Geophys. Res. Lett.* **40,** 3732–3737, doi: 10.1002/grl.50619.
Meschede, M. A., C. L. Myhrvold, and J. Tromp (2011). Antipodal focusing of seismic waves due to large meteorite impacts on Earth, *Geophys. J. Int.* **187,** 529–537, doi: 10.1111/j.1365-246X.2011.05170.x.
Press, W. H., S. A. Teukolsky, W. T. Vetterling, and B. P. Flannery (1992). Quick-and-Dirty Monte Carlo: The Bootstrap method, in *Numerical Recipes in C: The Art of Scientific Computing*, Second Ed., Cambridge University Press, Cambridge, United Kingdom, 994 pp.
Raveloson, A., R. Wang, R. Kind, L. Ceranna, and X. Yuan (2012). Seismic and acoustic-gravity signals from the source of the 2004 Indian Ocean tsunami, *Nat. Hazards Earth Syst. Sci.* **12,** 287–294, doi: 10.5194/nhess-12-287-2012.
Russian Ministry of Internal Affairs (2013). *Public Safety in the Chelyabinsk Region*, available at http://mvd.ru/news/item/845541/ (last accessed 6 September 2013) (in Russian).
Schiermeier, Q. (2013). The death of the Chebarkul meteor, *Nature* **495,** 16, doi: 10.1038/495016a.
Stone, D. (2013). Siberian meteor spurs dash for data, calls for safeguards, *Science* **339,** 1135, doi: 10.1126/science.339.6124.1135.
Tauzin, B., E. Debayle, C. Quantin, and N. Coltice (2013). Seismoacoustic coupling induced by the breakup of the 15 February 2013 Chelyabinsk meteor, *Geophys. Res. Lett.* **40,** 3522–3526, doi: 10.1002/grl.50683.
Wang, R. (2010). QSSP2010: FORTRAN code for calculating complete synthetic seismograms of a spherical Earth using the normal mode theory, available at http://www.gfz-potsdam.de/forschung/ueberblick/departments/department-2/erdbeben-und-vulkanphysik/services/downloads/ (last accessed 6 September 2013).
Wessel, P., and W. H. F. Smith (1998). New, improved version of the Generic Mapping Tools released, *Eos Trans. AGU* **79,** 579, doi: 10.1029/98EO00426.
Yeomans, D. (2013). *Fireball and Bolide Reports*, National Aeronautics and Space Administration, http://neo.jpl.nasa.gov/fireballs/ (last accessed 15 June 2013).

Sebastian Heimann
Álvaro González
Rongjiang Wang
Torsten Dahm
GFZ German Research Centre for Geosciences
Section on Earthquake Risk and Early Warning
Helmholtzstr. 7
14467 Potsdam, Germany
sebastian.heimann@gfz-potsdam.de

Simone Cesca
University of Potsdam
Institute of Earth and Environmental Science
Karl-Liebknecht-Str. 24-25
14476 Potsdam, Germany

Electronic Supplement to

Seismic characterization of the Chelyabinsk meteor's terminal explosion

by Sebastian Heimann, Álvaro González, Rongjiang Wang, Simone Cesca and Torsten Dahm

---

Waveform fits

These are the selected, high-quality displacement seismograms (28 vertical and 6 radial) of the Chelyabinsk meteor, recorded at 28 broadband seismic stations. They are shown, with normalized amplitude, in order of increasing epicentral distance. Recorded seismograms are in red, and modeled ones in blue. Each caption indicates the epicentral distance in km, network code (e.g., II), station code (e.g., ARU), "Z" for vertical seismograms and "R" for radial ones. The bottom axis shows the recording time (hours and minutes UTC). The origin time of the meteor's terminal explosion is indicated by red triangles.

Figure S1. Waveform fits.

Apparent Source-time Functions

The figure shows the apparent source-time functions for the Chelyabinsk's meteor terminal explosion. To look for systematic azimuthal variations in the waveform field, we deconvolved the observed seismograms with the synthetic ones for our best-fitting point-source solution in the frequency range 0.005 - 0.025 Hz. We used a water-level deconvolution technique, and stacked and normalized the station-wise results in 16 azimuthal bins (shown as columns). No significant azimuthal variation of the main pulse width can be observed (red stripes of similar width, at time 0), indicating that the explosion is well modeled as a point source in the frequency range used in our waveform-fitting procedure.

Figure S2. Apparent source-time functions.

Meteor’s Shock Wave Arrival in the Town of Korkino

The atmospheric shock wave of the meteor's terminal explosion needed almost a minute and a half to arrive to Korkino, the nearest town. This surveillance video was recorded inside Korkino's corrugated cardboard factory (YuzhUralKarton LLC, located at 61.347° E, 54.902° N). It is reproduced here by courtesy of the factory managers, thanks to the assistance of Mr. Dan Chernovalov. The direction of view is approximately towards NE. The moving meteor lights up the scene, mainly through the windows to the right. These are facing SSE (N 169° E, as measured in a map), towards the meteor trajectory. The extreme, apparent, peak brightness is reached 7.3 s after the start of this recording, and the shock wave arrives at 94.8 s, smashing the right-hand windows. We cannot measure the timing more accurately because of the slightly irregular frame rate. The observed delay of the shock wave (87.5 s after the meteor's explosion at peak brightness) is virtually identical to the one we calculated with our best-fitting explosion source (88 s).

Download/View: Video S1 [H.264-Encoded MP4; 8.5 MB]. Meteor’s light and delayed shock wave arrival at a factory in Korkino.

[Back]

Figure S1. Waveform fits.

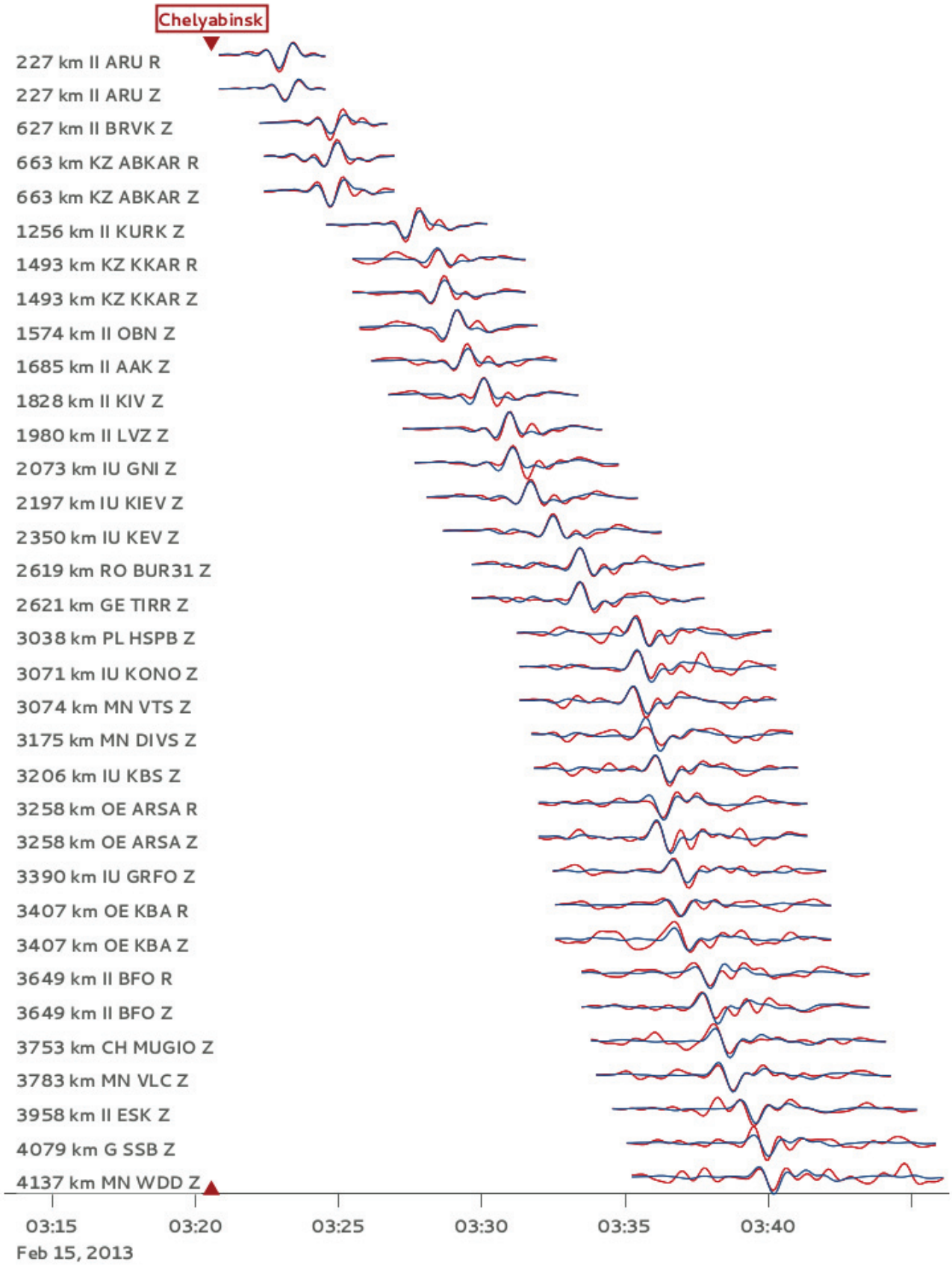

Figure S2. Apparent source-time functions.